

Journal of
Mechanics of
Materials and Structures

**STATISTICAL STRENGTH OF TWISTED FIBER BUNDLES WITH
LOAD SHARING CONTROLLED BY FRICTIONAL LENGTH
SCALES**

Pankaj K. Porwal, Irene J. Beyerlein and Stuart Leigh Phoenix

Volume 2, N° 4

April 2007



mathematical sciences publishers

STATISTICAL STRENGTH OF TWISTED FIBER BUNDLES WITH LOAD SHARING CONTROLLED BY FRICTIONAL LENGTH SCALES

PANKAJ K. PORWAL, IRENE J. BEYERLEIN AND STUART LEIGH PHOENIX

We develop Monte Carlo simulation and theory to study the statistical strength characteristics of twisted fiber bundles. These consist of fibers that follow a Weibull distribution for strength with shape parameter ρ , and are arranged in an ideal helical structure with surface helix angle α_s . Fiber interactions are considered in terms of frictional forces that control stress recovery along broken fibers away from the breaks. A twist-modified global load sharing (TM-GLS) rule is developed for stress redistribution from fibers that are slipping and thus only partially loaded near the breaks. Expressions for the radial pressure distribution in the yarn and corresponding lengths of frictional zones in broken fibers in the various layers are derived considering the discrete nature of the fibers in the bundle. Three different characteristic length scales of strength development for a twisted bundle are proposed, which depend on friction coefficient, f , and surface twist angle, α_s . These are δ_c^{\min} , δ_c^{avg} , or δ_c^{\max} , arising from the consideration of the minimum, average, or maximum stress recovery length among the fibers in the bundle along its axis. We show that the normalized strengths of a twisted bundle with length equal to any one of these characteristic lengths approximately follow a Gaussian distribution. Compared to a TM-ELS (twist-modified equal load sharing) bundle, the TM-GLS bundle has improved strength because through friction a broken fiber can recover its stress within the bundle length. We also show that the relationship between the normalized bundle strength and α_s depends on the characteristic length scale used: for δ_c^{\min} the normalized strength drops quickly with α_s ; for δ_c^{avg} it decreases as well, but at a slower rate; and for δ_c^{\max} the normalized strength first attains a maximum at an optimal value of α_s before ultimately decreasing with α_s . Finally, we compare the simulation results for optimal twist angle with experimental data in the literature and get excellent agreement.

1. Introduction

Twisted fibrous structures, such as ropes and cables made from ultrastrong fibers like Kevlar[®], Spectra[®], Dyneema[®], and Vectran[®], are now used in a wide range of applications requiring not only very high tensile strength and stiffness but also flexibility in bending. Novel applications are emerging from commercialization of fibers like M5[®] (DuPont) and synthetic spider silk [Lazaris et al. 2002; Huemmerich et al. 2004]. Still others in development are based on aligned and twisted carbon nanotube bundles

Keywords: twisted fiber bundle or yarn, Monte Carlo simulation, statistical strength, global load sharing, characteristic length scales, friction effects, pressure development.

The authors would like to gratefully acknowledge the support of the Science- and Technology-based Distinguished Student Award provided to graduate student Pankaj K. Porwal by Los Alamos National Laboratory. IJB and PKP would like to thank the Fluid Dynamics Group (T-3) management and administration for their support. This work has been supported in part under the "Institute for Future Space Transport", a NASA University Institute funded under Cooperative Agreement NCC3-994. This research was conducted using the resources of the Cornell Theory Center, which receives funding from Cornell University, New York State, federal agencies, foundations, and corporate partners.

[Andrews et al. 1999; Vigolo et al. 2000; Jiang et al. 2002; Ko et al. 2003; Ericson et al. 2004; Zhang et al. 2004]. These novel applications include, but are not limited to, linear structures (for example, suspension ropes in bridges, parachute lines, tire cords, and the futuristic concept of the *space elevator*), and two-dimensional fabric-based structures (for example, body armor in the form of ballistic vests, blankets, and panels in automobiles and aircrafts). In many of these critical applications, survival of the user depends upon the optimal functioning of the twisted structure, and in such cases reliable strength predictions are crucial.

The most common model geometry for a twisted fiber bundle or yarn is the ideal helical structure [Hearle et al. 1969], in which the fibers are arranged in concentric layers following helical paths with the same angular orientation. The outermost layer has the highest helix angle (that is, the surface helix angle α_s) and layers deeper into the bundle have progressively lower helix angles down to the center fiber which is straight. Furthermore, fibers in this ideal structure have no initial strains or buckling, which requires that fibers in different concentric layers have lengths equal to the helical path lengths of their particular layer. In practise, achieving this uniformity in a long yarn that has been twisted in an automated manufacturing process, requires the phenomenon of *migration*. During migration fibers, traveling along the yarn length, radially move from one layer to another over length scales that are long compared to both the yarn diameter and the characteristic length of stress transfer near fiber breaks. When such an ideal helical structure is under an external tensile load, the fiber strains are largest along the yarn axis and smallest in the outermost layer.

1.1. Optimal strength of yarn. Earlier works predicting the strength of ideal yarns have focused mostly on staple yarn structures where fibers are of a given finite length and deterministic strength. For a given coefficient of interfiber friction and surface twist angle the strength of the yarn, also deterministic, is governed by the first fiber to fail, this being the center fiber. Additional strain increments cause a cascade of fiber failures propagating outwards until the complete collapse.

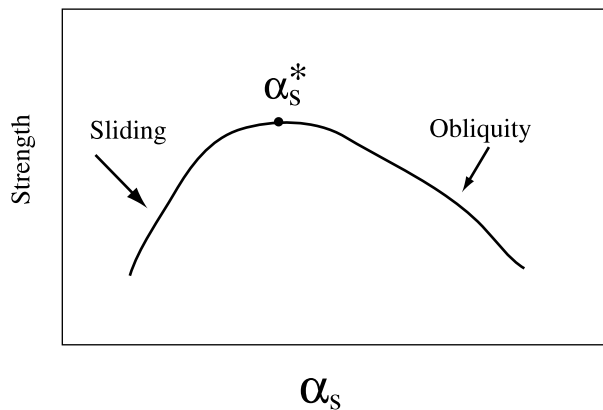


Figure 1. Staple yarn strength versus surface helix angle. Optimal helix angle exists due to the strengthening effects of yarn pressure and interfiber friction, and to the weakening effects of fiber obliquity as the surface helix angle is increased.

Twisting of a yarn produces both strengthening and weakening influences. This is illustrated in Figure 1, which is a plot of yarn strength versus surface helix angle. At low helix angles, as the surface helix angle increases the radial pressure in the yarn also increases causing more rapid stress recovery along fibers near breaks leading to overall strengthening of the yarn. At higher twist angles, obliquity effects in the fibers become dominant, since the fiber stress component contributing to the strength is proportional to the square of the cosine of the helix angle of the fiber path. Overall the sum of all stress components decreases as the surface helix angle is increased. Because of these two competing effects there exists a twist level, called optimal twist, where the maximum yarn strength is achieved. The optimal twist level and the maximum strength also depend on various constituent properties. For an excellent summary of the earlier theoretical and experimental works, we refer the readers to [Hearle et al. 1969].

1.2. Weibull fiber strength. High-performance fibers like Kevlar, Spectra, and even CNTs [Barber et al. 2005] exhibit statistical variation in their strength or strain to failure, which is typically described by a statistical distribution also involving length effects. Due to this variation, failure of the parent yarn is a stochastic process dictated by the stress field and sampling of fiber strengths along the yarn. This complex failure process imparts statistical variation and size effects to yarn strength.

The Weibull distribution is commonly used to describe the statistical variation in fiber strength giving the probability of failure of a fiber at stress level σ as

$$F(\sigma) = 1 - \exp \left\{ - \left(\frac{\sigma}{\sigma_{\delta_0}} \right)^\rho \right\},$$

where σ_{δ_0} and ρ are Weibull scale and shape parameters. Note that the scale parameter σ_{δ_0} corresponds to length δ_0 of the fiber (corresponding to a standard gauge length used in tension tests). For an arbitrary fiber length δ the scale parameter can be modified as [Phoenix and Beyerlein 2000]

$$\sigma_\delta = \left(\frac{\delta_0}{\delta} \right)^{1/\rho} \sigma_{\delta_0}, \tag{1}$$

and the probability of failure at stress level σ corresponding to fiber length δ is given by

$$F(\sigma) = 1 - \exp \left\{ - \frac{\delta}{\delta_0} \left(\frac{\sigma}{\sigma_{\delta_0}} \right)^\rho \right\}. \tag{2}$$

1.3. Load sharing among broken fibers. When a fiber breaks, the load that it previously carried is redistributed among the intact fibers. Historically, several idealized load sharing rules, for example, equal load sharing (ELS), global load sharing (GLS), and local load sharing (LLS), have been developed for parallel (untwisted) bundles.

In ELS the load from a broken fiber is lost along the full fiber length between the clamps and is redistributed equally among the intact fibers. In GLS the load from a broken fiber is locally lost at the break but is gradually recovered over length l_f away from the break through interfiber frictional shear forces. The full length of the recovery region is $2l_f$ and is called the recovery zone. At any cross-section intersecting the recovery zone of a break, the difference between the fiber stress before the break occurred and that actually supported by the fiber in presence of the break is distributed equally among the intact, nonslipping fibers in that cross-section. In LLS the lost load from a broken fiber is locally redistributed among its nearest neighbors according to various possible rules.

In a twisted yarn the primary factors in the construction of the load sharing rule are sliding interfiber friction near fiber breaks and the length scales they introduce as well as fiber obliquity due to twist. These are affected by surface helix angle, radial position in the yarn, and yarn tension. Attempts to account for some of the above features have appeared in the literature. Pan [1993] developed an orientation efficiency factor that he applied to Daniels' ELS bundle strength. Otherwise the ELS rule applied to all the fibers in the bundle. Pan et al. [1998] and Rao and Farris [2000] performed some experiments to show the existence of optimal strength and size effects in the yarns. On the other hand, Phoenix [1979] modeled twisted fiber bundle with Weibull fibers incorporating slack effects resulting from incomplete migration but ignored friction.

Recently Porwal et al. [2006] developed a Monte Carlo simulation model for the failure of a twisted bundle to assess the accuracy of two simplified analytical models, one based on geometrical averaging and the other on statistical averaging. The simulation model made use of a new load sharing rule, called twist-modified equal load sharing (TM-ELS), which is an extension of the ELS rule and accounts for the effects of twist but ignores friction. Under TM-ELS equilibrium is satisfied only in the yarn axis direction. The Monte Carlo simulation model as well as the two analytical theories resulted in the yarn strength being normally distributed. Very good agreement was found between the two theories and the simulation results for a wide range of yarn surface helix angles and variability in fiber strength as measured by the Weibull shape parameter. Favorable comparison was also achieved between the results of Porwal et al. [2006] and Phoenix [1979]. Finally Porwal et al. [2006] considered the issue of interfiber friction; its effect on fiber stress transfer and ultimately on the strength of a long yarn was treated in a simplified way in a chain-of-bundles model. Other more recent attempts in this category, including work on impregnated yarns, are by Naik et al. [2001] where they estimated strength of impregnated yarn using effective shear traction and fiber obliquity factor.

In the current work a probability model for the strength of a twisted bundle with an ideal helical structure is developed, which accounts for statistical Weibull fiber strength and frictional effects. To do so, we first develop a new load sharing rule, called the twist modified global load sharing (TM-GLS) rule. Specifically, TM-GLS is an extension of GLS similar to the extension of ELS to obtain TM-ELS as in [Porwal et al. 2006], applied over small yarn division.

1.4. Characteristic length for the bundle. The aim of the current work is to compare TM-ELS and TM-GLS simulations and observe the effects of friction on the bundle strength distribution and also the size effects. Such extension from TM-ELS to TM-GLS is nontrivial because it involves not only accounting for a radial pressure distribution in the context of a changing fiber stress distribution as fibers fail, but also an extension from two dimensions (a cross-sectional plane) to three dimensions, where the third dimension is a characteristic frictional length. For an individual fiber, the characteristic length is usually defined as the fiber length over which slipping occurs around a break [Phoenix and Beyerlein 2000]. This length will vary from fiber to fiber depending on its helix angle and frictional forces on its surface. To simulate the strength of a bundle it is necessary to choose a bundle length that effectively captures the characteristic stress transfer lengths of the constituent fibers. To this end we examine three specific choices of the bundle simulation lengths in this work and find that it has a strong influence on the capacity of the individual fibers in the yarn to develop the maximum stress determined by yarn extension as well

as to have multiple breaks along its length. For only one of these choices the bundle stress achieves a maximum.

2. Modeling approach

We consider the same yarn geometry as used in the previous work by Porwal et al. [2006] and thus only review the main points. In this work we do not consider effects such as twisting caused by the yarn tensile load or torque caused by the yarn tensile strain. The twisted bundle has n fibers, which are concentrically packed in l layers as shown in Figure 2. Fibers form concentric layers with the assumption that if there is a large enough void in the concentric layer for a fiber, then it is occupied by the fiber. The layers are numbered $1, \dots, k, \dots, l$. The midpoint of layer k is located at a radius r_k from the yarn axis and is given by $r_k \approx (k - 1)d_f$, where d_f is fiber diameter. Also the helix angle α_k of the fibers in layer k is given as

$$\alpha_k = \tan^{-1} \frac{r_k \tan \alpha_s}{R},$$

where $R = r_l$ is the yarn radius and α_s is the helix angle of the outermost layer l . The number of concentrically accommodated fibers in layer k is given by

$$n_k \approx \left\lfloor \frac{2\pi(k - 1)d_f}{d_f} \right\rfloor \approx \lfloor 2\pi(k - 1) \rfloor \approx 2\pi(k - 1), \quad \text{for } k > 1 \text{ and } n_1 = 1,$$

where $\lfloor \cdot \rfloor$ is the floor function. Note that n_k does not depend on d_f and $n = n_1 + \dots + n_l$ is the total number of fibers in the yarn.

2.1. Development of tension from free ends. The distinct feature of a GLS bundle is the gradual recovery of stress in a fiber away from breaks. Consider a fiber section of length L between two breaks in layer k . If fP_k is the frictional force per unit area on the lateral surface of a sliding fiber element in this section (Figure 3), where f is the coefficient of friction and P_k is the interfiber contact pressure on layer k acting normal to the fiber surface, then from the equilibrium along the fiber length we have $dT'_k(\pi d_f^2/4) = fP_k\pi d_f dx$. The tensile stress in the fiber in terms of distance x along the fiber axis from

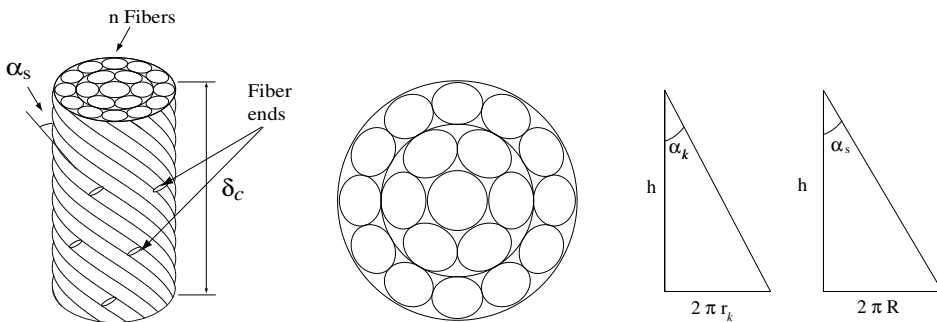


Figure 2. Yarn geometry: (left) yarn segment, (middle) concentric packing, (right) layer helix angles, where h is the height of one turn of twist.

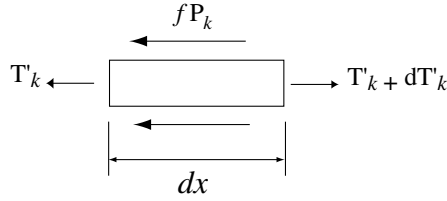


Figure 3. Development of tension in the fiber near a break in layer k .

a break is given by

$$\frac{dT'_k}{dx} = \frac{4fP_k}{d_f}, \quad \text{for } 0 \leq x \leq l_{f_k}, \tag{3}$$

where $l_{f_k} \leq L/2$ is the length of the friction zone on either end of the fiber. Using the boundary condition $T'_k = 0$ at $x = 0$, Equation (3) integrates to

$$T'_k(x) = \frac{4fP_k}{d_f}x, \quad \text{for } 0 \leq x \leq l_{f_k}. \tag{4}$$

From Equation (4) the maximum tensile stress T_k in a fiber, first attained at $x = l_{f_k}$, is given by

$$T_k = \frac{4fP_k}{d_f}l_{f_k}. \tag{5}$$

The fiber is called a nonslipping fiber if the stress given by Equation (5) is equal to the stress determined by yarn extension, neglecting Poisson’s effect [Hearle et al. 1969], that is,

$$T_k = E_f \epsilon_y \cos^2(\alpha_k), \tag{6}$$

where ϵ_y and E_f are the yarn strain and fiber Young’s modulus, respectively. In this case there are two distinct friction zones in a fiber at the ends with the tensile stresses linearly increasing from 0 to T_k . Over the middle portion of length $L - 2l_{f_k}$ the tensile stress remains equal to T_k , which is considered effectively gripped as depicted in Figure 4 with a solid line. For such a fiber the average tensile stress can be written as

$$\bar{T}_k = \frac{1}{L} \left(2l_{f_k} \frac{T_k}{2} + T_k(L - 2l_{f_k}) \right) = T_k \left(1 - \frac{l_{f_k}}{L} \right). \tag{7}$$

Otherwise, for the slipping fiber, the maximum developed tensile stress from Equation (4) will be just $2fP_kL/d_f$ for $l_{f_k} = L/2$. In this case two friction zones of length $L/2$, as depicted by the dashed line in Figure 4, are symmetrically placed about the center with zero stress at the ends and maximum stress, $2fP_kL/d_f$, in the middle. The average stress in this case thus will be

$$\bar{T}_k = \frac{fP_k}{d_f}L. \tag{8}$$

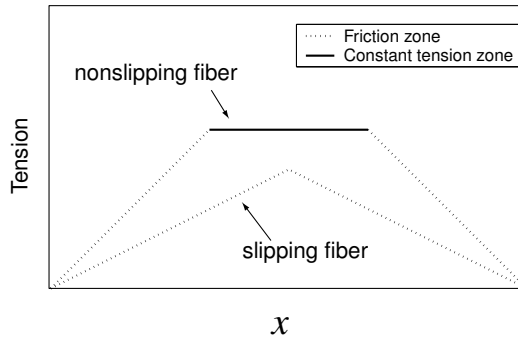


Figure 4. Tensile stress profiles in the fibers.

2.2. Pressure calculations. In this section we develop an expression for interfiber contact pressure as a function of radial distance in a yarn cross-section considering the discrete nature of the fibers in the yarn. We begin by considering the pressure developed by a single fiber helically wrapped around a cylinder under tension.

2.2.1. Pressure developed by an individual fiber. When a fiber under constant tension T is wound around a cylinder in a circular loop a nominal contact pressure P is experienced by both the fiber and cylinder given by

$$P = \frac{dT}{r} = \frac{d_f T}{r}, \tag{9}$$

where r is the radius of cylinder and d is the nominal contact width along the fiber. To simplify the pressure calculation we assume that the fiber has a square cross-section with side d_f so that $d = d_f$.

In the case of a twisted bundle, the above expression needs to be modified to account for the helical path of the fiber (Figure 5). This can be easily done by replacing r in the denominator of Equation (9)

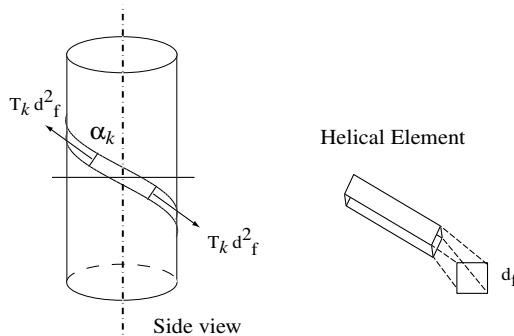


Figure 5. Pressure developed by a helically wound fiber in the k -th layer (left). The fiber cross-section is assumed to be square for the purpose of calculating pressure (right).

by the local radius of curvature, which is $r_k / \sin^2 \alpha_k$. Thus the pressure developed becomes

$$P_{k,k} = \frac{d_f T_k \sin^2(\alpha_k)}{r_k}. \tag{10}$$

This pressure acts normal to the lateral surface of the fiber and is assumed to be constant across the entire cross-section of the fiber. It is clear from Equation (10) that as the helix angle increases, the pressure developed by the fiber increases.

The above expression for pressure assumes that the stress in the fiber is constant along the length of the fiber. However, this is not the case in an actual yarn. To account for the effect of varying stress in the fiber we use an average stress \bar{T}_k over the length of the fiber to calculate the average pressure, that is,

$$\bar{P}_{k,k} = \frac{d_f \bar{T}_k \sin^2(\alpha_k)}{r_k}, \tag{11}$$

where \bar{T}_k is given by either Equation (7) or (8). Henceforth the average pressure is simply called the pressure.

2.2.2. Pressure variation in the yarn. For layer k within the yarn the total pressure \bar{P}_k is sum of its own pressure, Equation (11), and the pressure from layers outside it. To ease the calculation of the pressure in layer k we assume that the fibers inside and outside of this layer are homogeneous isotropic cylinders. Thus, the pressure is given by

$$\bar{P}_k = \bar{P}_{k,k} + \bar{P}_{k,o} = \sum_{j=k}^l \bar{P}_{j,j}, \tag{12}$$

where $\bar{P}_{k,o} = \sum_{j=k+1}^l \bar{P}_{j,j}$ is the contribution to the pressure from layers outside the k -th layer.

Note that calculation of the pressure using discrete fibers allows us to account for individual fiber failures. This, however, is beyond the scope of this work and left for a future study.

2.3. Lengths of friction zones in fiber. We consider the two cases corresponding to the two fiber stress profiles in Figure 4.

Case 1: nonslipping fiber. This case considers the nonslipping fiber in Figure 4. If the pressure in layer k is \bar{P}_k , then Equation (5) would become

$$T_k = \frac{4f \bar{P}_k}{d_f} l_{f_k}. \tag{13}$$

From Equations (12) and (13) we obtain

$$T_k = \frac{4f}{d_f} (\bar{P}_{k,k} + \bar{P}_{k,o}) l_{f_k}, \tag{14}$$

and using Equations (6), (7), (11) and (14) we get

$$\frac{d_f \cos^2(\alpha_k)}{4f} = \left[\frac{d_f \cos^2(\alpha_k) \sin^2(\alpha_k)}{r_k} \left(1 - \frac{l_{f_k}}{L} \right) + \frac{\bar{P}_{k,o}}{E_f \epsilon_y} \right] l_{f_k}. \tag{15}$$

Defining C_k and B_k as

$$C_k = \frac{d_f \cos^2(\alpha_k) \sin^2(\alpha_k)}{r_k}, \quad B_k = \frac{d_f \cos^2(\alpha_k)}{4f},$$

we can solve Equation (15) to obtain l_{f_k} as

$$l_{f_k} = \frac{(C_k + \bar{P}_{k,o}/E_f \epsilon_y) - \sqrt{(C_k + \bar{P}_{k,o}/E_f \epsilon_y)^2 - 4C_k B_k/L}}{2C_k/L}$$

$$= \frac{L}{2} \left\{ \left(1 + \frac{\bar{P}_{k,o}}{C_k E_f \epsilon_y} \right) - \sqrt{\left(1 + \frac{\bar{P}_{k,o}}{C_k E_f \epsilon_y} \right)^2 - \frac{r_k}{fL \sin^2(\alpha_k)}} \right\}. \tag{16}$$

Here we consider only the negative solution because the positive solution gives $l_{f_k} > L/2$.

Case 2: slipping fiber. For the case of the slipping fiber in Figure 4, Equations (8), (11), and (12) yield

$$\bar{P}_{k,k} = \frac{f \bar{P}_k L \sin^2(\alpha_k)}{r_k} = \frac{f(\bar{P}_{k,k} + \bar{P}_{k,o})L \sin^2(\alpha_k)}{r_k},$$

giving

$$\bar{P}_{k,k} = \frac{\bar{P}_{k,o}}{\frac{r_k}{fL \sin^2(\alpha_k)} - 1}. \tag{17}$$

Since the layers cannot make a negative pressure contribution, the denominator of the Equation (17) must be positive, that is,

$$\frac{r_k}{fL \sin^2(\alpha_k)} > 1.$$

This requirement is opposite the condition required for the validity of Equation (16), which is

$$\frac{r_k}{fL \sin^2(\alpha_k)} < \left(1 + \frac{\bar{P}_{k,o}}{C_k E_f \epsilon_y} \right)^2 \quad \text{or} \quad \frac{r_k}{fL \sin^2(\alpha_k)} < 1^+,$$

where 1^+ is any quantity > 1 . The friction zone length for this case will be $l_{f_k} = L/2$.

Note that for the l -th layer, which is the outermost layer, $\bar{P}_{l,o} = 0$ by definition. Furthermore, if case 2 is true, then it is a degenerate case 2 because no pressure development means zero tension in the fibers. This leads to $\bar{P}_l = 0$ and so on for all other layers and by our assumptions thus far the fibers will simply unravel. To overcome this difficulty we can assume some nonzero external pressure $P_o > 0$ as Sullivan [1942] did. Also note that in an actual yarn, fibers do not stay in one particular layer over the whole yarn length, but they rather move from layer to layer through the process called migration. Consequently, despite having several breaks, a surface fiber can be well anchored over much of its length thus allowing tension and hence pressure to develop.

2.4. Characteristic lengths of bundle for strength calculation. Here we define three different characteristic length scales based on constituent material and yarn geometrical properties, which are crucial to strength development in the yarn with each one involving a different failure mechanism. The axial length of the yarn that will develop the maximum tension (as determined by yarn extension) from a single break

in the cross-section passing through the middle of the yarn length in layer k is $2l_{f_k} \cos \alpha_k$. Three length scales δ_c^{\max} , δ_c^{\min} , and δ_c^{avg} can be computed from this length

$$\delta_c^{\max} = \max_k \{2l_{f_k} \cos \alpha_k\}, \quad \delta_c^{\min} = \min_k \{2l_{f_k} \cos \alpha_k\}, \quad \delta_c^{\text{avg}} = \sum_{k=1}^l w_k 2l_{f_k} \cos \alpha_k.$$

The last definition uses a weight function w_k , a suitable choice of which is the fraction of fibers in each layer, that is, $w_k = n_k/n$. Taking $\delta_c = \delta_c^{\max}$ all fiber layers can reach maximum tension if a break develops in the cross-section passing through the middle of the yarn length. In other words, through the frictional stresses, the axial tension is recovered far from the break point to the level that the fiber can sustain redistributed stress. In the case of $\delta_c = \delta_c^{\min}$, only the layer with the minimum length of friction zone projected along the yarn axis can develop maximum tension along their broken fibers. So in this case frictional stresses are largely unutilized. For $\delta_c = \delta_c^{\text{avg}}$, only some of the broken fibers can develop maximum tension, utilizing frictional stresses moderately.

2.5. TM-GLS and Monte Carlo simulation algorithm. In the Monte Carlo simulation model we consider a characteristic length δ_c of the yarn. Since it is not feasible to redistribute the load at each cross-sectional plane, we divide this characteristic length into a predetermined number n_{div} of divisions of much shorter length $\delta = \delta_c/n_{\text{div}}$. Because of the helical paths of the fibers, the fiber elements in layer k actually have longer lengths $\delta_k = \delta/\cos \alpha_k$, which also differs from layer to layer. We then assign a random strength $X_{f,i}^{\text{div}}$ to each fiber element in the yarn characteristic length, where i is fiber number and div is the division number that ranges from 1 to n_{div} . These strengths are assigned according to a Weibull distribution whose shape parameter is ρ and the scale parameter is referenced to length δ_k for layer k according to Equation (2) with $\delta = \delta_k$.

The TM-GLS redistribution scheme evolves iteratively using the following discrete steps as we increase the external load, keeping in mind that after any particular step a given fiber may have one or more breaks:

- (i) In a particular step t the axial stresses of the fiber elements are first calculated and then compared to the assigned fiber element strengths $X_{f,i}^{\text{div}}$.
- (ii) From this comparison any fiber element whose axial stress exceeds its assigned strength is considered failing in this step in which case its load becomes zero. The stresses in all other elements along this fiber that are in the stress recovery zone of this newly broken element are then calculated according to

$$T_{f,i}^s = \frac{4f}{d_f} \bar{P}_k c \delta_k, \quad \text{if } \frac{4f}{d_f} \bar{P}_k c \delta_k \leq T_{f,i},$$

where $T_{f,i}$ is the stress in the individual fiber i as determined by yarn extension and integer c is the distance of a particular element from the broken element in terms of number of elements, that is, for the broken fiber element $c = 0$ and for subsequent neighboring elements $c = 1, 2, \dots$ on either side of the newly broken element. When there are breaks on both sides of an unbroken element, then c must be modified to be the smaller of two values obtained by counting from each of the broken elements. The elements just described are slipping elements in the recovery zone of some broken

element and thus have stresses less than $T_{f,i}$. Thus, they are actually shedding stresses that are then resolved along the yarn axis.

- (iii) These resolved components are then redistributed equally to the stress components (resolved along the yarn axis) of the fiber elements not shedding their stresses, and then the stresses of these elements acting along their own respective axes are recalculated.
- (iv) The stresses in the recovery zones of newly broken elements are then set equal to the stresses determined in Section 2.5 (ii).

Our general scheme is to model the failure process in discrete steps $t = 0, 1, \dots$ in the following way. (To simplify the notation we suppress the superscript *div* in $T_{f,i}^{s(\text{div})}$). At step t we denote the stress in fiber element i acting along its own axis (not the yarn axis) as $T_{f,i}^{(t)}$ as in (i) above. $T_{f,i}^{(t)}$ is considered to be composed of two components: the first is the stress carried by the fiber element $T_{f,i}^{\epsilon(t)}$ due to the applied load as if all the fibers are intact, while the second is the sum of the additional stress portions inherited from the fiber elements shedding their stresses $T_{f,i}^{r(t)}$ in that division. Summing these for fiber element i within a particular yarn division we have

$$T_{f,i}^{(t)} = \begin{cases} T_{f,i}^{s(t)}, & \text{if fiber is shedding its stress,} \\ T_{f,i}^{\epsilon(t)} + T_{f,i}^{r(t)}, & \text{otherwise.} \end{cases}$$

From Equation (6) for fiber element i we have $T_{f,i}^{\epsilon(t)} = E_f \epsilon_y \cos^2 \alpha_{f,i}$. At each step we recalculate $T_{f,i}$ according to

$$T_{f,i}^{(t+1)} = \begin{cases} T_{f,i}^{s(t+1)}, & \text{if fiber is shedding its stress,} \\ T_{f,i}^{\epsilon(t+1)} + T_{f,i}^{r(t)} + \frac{\sum_{j=1}^{n_b} (T_{f,b(j)}^{(t)} - T_{f,b(j)}^{s(t+1)}) \cos \alpha_{f,b(j)}}{(n - N_b) \cos \alpha_{f,i}}, & \text{otherwise,} \end{cases}$$

where $b(j)$ is the index number of j -th fiber element shedding its load, n_b is the number of additional fiber elements shedding their loads when going from step t to $t + 1$, and N_b is the total number of fiber elements shedding their loads at $t + 1$. In this equation we see a stress enhancement effect in the benefactor fiber (along its axis) that results when it has a larger helix angle as compared to the fiber that failed.

We note that t does not necessarily correspond to an increment in the applied loading; the index t is increased either (a) when we increase the external load level, or (b) when at a given external load level the redistribution of stresses leads to failure of more fibers.

At any step t the applied stress is in equilibrium with internal stresses developed by the fiber elements in each division, so the stress carried by the yarn is given by

$$\sigma^{(t)} = \frac{\sum_{i=1}^n T_{f,i}^{(t)} \cos(\alpha_{f,i})}{\sum_{i=1}^n 1 / \cos \alpha_{f,i}}$$

and the strength of the yarn would be $\max_t \{\sigma^{(t)}\}$. We note one fundamental difference between TM-GLS and GLS. In the latter once a fiber element falls in the friction zone, its stress remains constant during further external load increments; so it can not fail. In the former, however, stresses in slipping fiber elements may increase due to the ever increasing yarn pressures and frictional forces.

3. Results and discussion

We normalize the bundle strength and failure behavior quantities with σ_{δ_c} , the Weibull scale parameter corresponding to the yarn characteristic length δ_c . Since there are no stiffness variations in the fibers and no interfiber slack effects inherited from the migration, the actual fiber Young’s modulus and Weibull scale parameter for fiber strength are normalized out of the calculation. Note that σ_{δ_c} depends on δ_c and ρ through Equation (1). In the simulations the key parameter ρ is varied from 2 to 10. This range is typical of commercially available high-performance fibers such as Toray carbon T1000G, Kevlar, Spectra, Zylon, with diameters on the order of 4 to 25 μm . Another key parameter is the interfiber friction coefficient f which affects δ_c (see Figure 9). We consider the values $f = 0.1$ and 0.3, which are representative of the above mentioned fibers. All of the following simulations are for $\delta_c = \delta_c^{\min}$ unless stated otherwise. We also vary the surface twist angle over $0^\circ < \alpha_s < 25^\circ$. The normalized value of external pressure is assumed to be $\bar{P}_{l,0}/E_f\epsilon_y = 0.001$ or 0.1% of the fiber stress in an untwisted yarn, which is a small fraction of the pressure typically generated even for small twist angles as seen later. The fiber diameter is taken as $d_f = 10 \mu\text{m}$ and the length of fiber in the simulation is $L = 20 \text{ cm}$. Typically this length is longer than the fiber characteristic length at very small twist because of the initial external constraining pressure.

3.1. Convergence study. We first study the convergence of μ/σ_{δ_c} for important simulation parameters such as the number of replications n_s , number of divisions n_{div} , and magnitude of stress increment ΔT . To achieve sufficient accuracy in the simulations we determine acceptable values of these parameters in an iterative manner. First we fix $n_{\text{div}} = 50$ and $\Delta T = E_f\Delta\epsilon$, where $\Delta\epsilon = 0.001$ is much smaller than the Weibull scale parameter for fiber failure strain, and find the value of n_s for which we get convergence. Figure 6 (left) shows a plot of the normalized mean μ/σ_{δ_c} versus number of replications. We find very good convergence for n_s beyond 200. Next we fix $n_s = 500$ and $n_{\text{div}} = 50$ and study μ/σ_{δ_c} versus strain increment, $\Delta\epsilon$, that is, $\Delta T = E_f\Delta\epsilon$. Figure 6 (right) shows the resulting convergence for decreasing

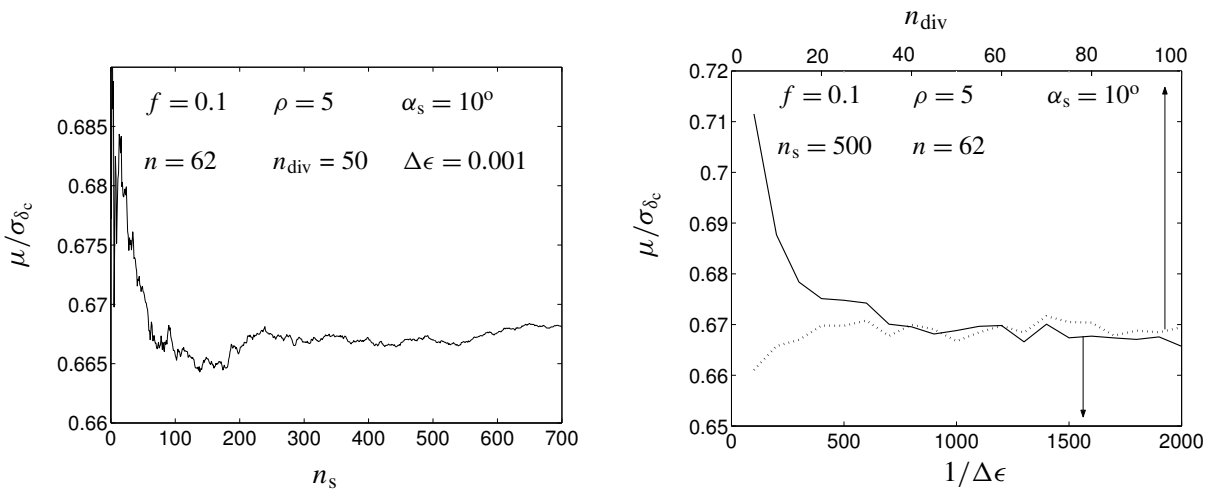


Figure 6. Convergence of normalized mean, μ/σ_{δ_c} , versus (left) number of runs, n_s , and (right) number of divisions, n_{div} , and strain increment, $\Delta\epsilon$.

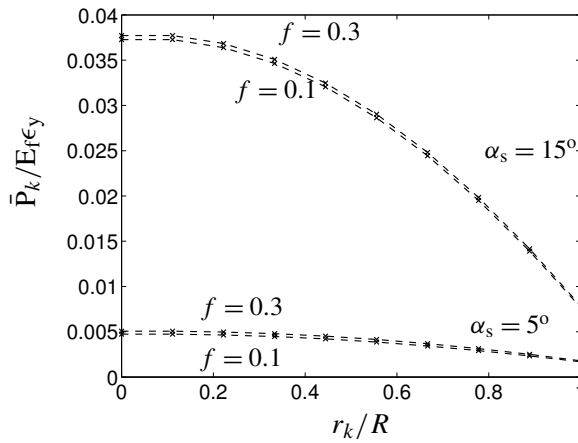


Figure 7. Normalized pressure, $\bar{P}_k/E_f\epsilon_y$, versus normalized radial distance, r_k/R . Here $l = 10$ and $n = 279$.

$\Delta\epsilon$. We also fix $n_s = 500$ and $\Delta\epsilon = 0.001$ and consider the convergence of μ/σ_{δ_c} in n_{div} , also shown in Figure 6 (right). Thus we choose $n_s = 500$, $n_{div} = 50$ and $\Delta\epsilon = 0.001$ for our simulations.

3.2. Pressure development, fiber friction zone and yarn characteristic lengths. Figure 7 shows the change in normalized pressure with normalized radial distance from the center of the yarn. The pressure increases as radius decreases to the center of the yarn, whereby the pressure contributions of the outer layers accumulate. The calculation in Figure 7 considers all the fibers to be intact. For this reason there is little difference in pressure distribution for the different friction coefficients $f = 0.1$ and 0.3 (for both $\alpha_s = 5^\circ$ and 15°). Fibers that fail carry reduced stresses over the characteristic fiber and yarn lengths leading to an overall decrease in pressure magnitude from that shown in Figure 7. Friction will also

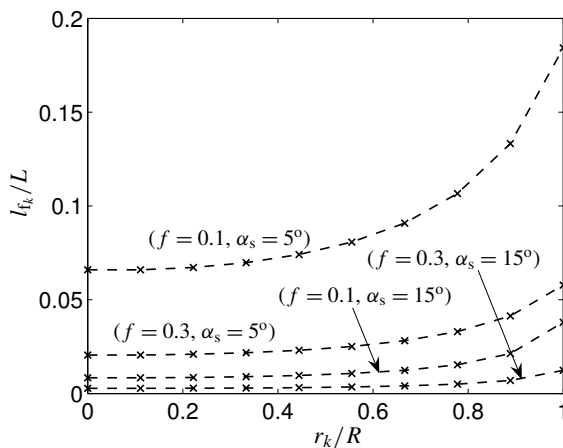


Figure 8. Normalized friction length, l_k/L , versus normalized yarn radius, r_k/R . Here $l = 10$ and $n = 279$.

come into play after a significant number of fiber breaks have accumulated in the yarn. In Figure 7 we note a huge gain in pressure with increase in α_s . This happens because of the effect of sine-squared of the helix angle in the numerator of Equation (10).

Figure 8 shows plots of the friction zone length versus radial distance from the center of the yarn. As anticipated, the friction length increases from the center to the outer surface irrespective of f and α_s . For a fixed α_s the length of the fiber friction zone decreases with increasing f and for a fixed f it decreases with increasing α_s . As is the case for the pressure distribution in the yarn, the α_s has a stronger effect than f on the fiber friction zone length.

The marker points in Figures 7 and 8 correspond to the values at the centers of the concentric layers and dashed lines are there to show the trend.

Figure 9 shows the decrease in the three characteristic length scales, which we consider in this work, with α_s for $f = 0.1$. The reduction occurs because the friction lengths decrease with an increase in α_s . As expected, $\delta_c^{\max} > \delta_c^{\text{avg}} > \delta_c^{\min}$ for all α_s . Also, we see the same trend for other values of coefficient of friction.

3.3. Stress strain curves. Figure 10 shows sample stress strain curves corresponding to different values of the Weibull shape parameter, ρ , and surface helix angle, α_s . The simulation assumes a stress-controlled tensile experiment. The lower, isolated marker points indicate sudden collapse of the yarn. We define the strain ϵ_y in Figure 10 as the strain in the intact virtual central fiber of the yarn. Therefore the slope of these curves is a reasonable approximation of yarn elastic stiffness. The linearity of all the curves until sudden failure suggests a macroscopic brittle-like behavior. For a fixed α_s the slope increases with an increase in ρ , whereas in the case when ρ is fixed the slope decreases with an increase in α_s . Also

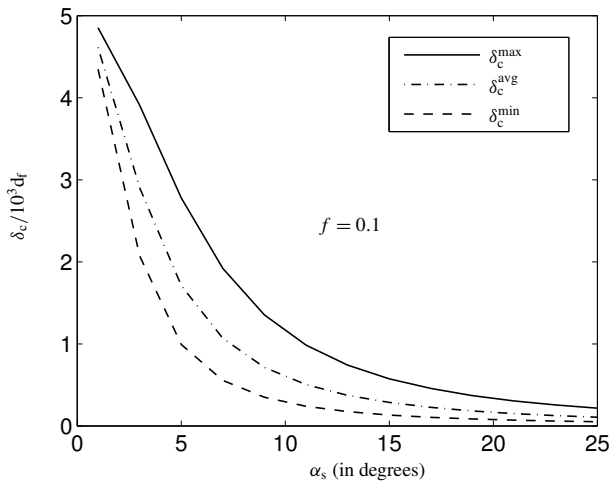


Figure 9. Normalized characteristic length scale for strength development $\delta_c / 10^3 d_f$ versus surface helix angle α_s . $l = 10, n = 279$.

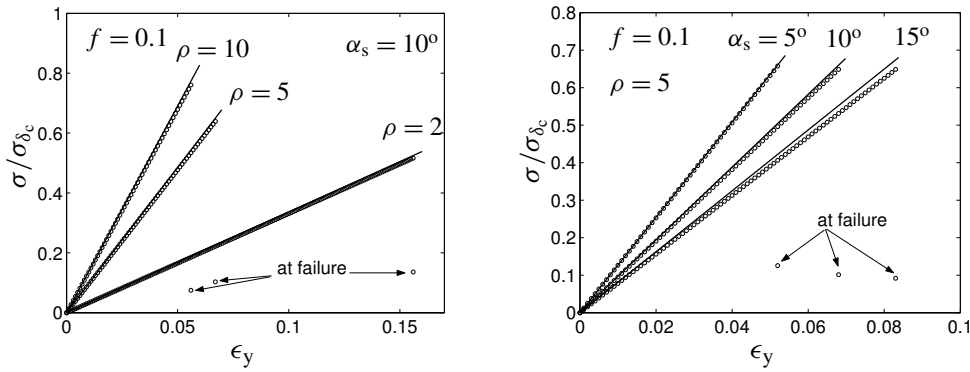


Figure 10. Stress strain curves for twisted yarn for various parameters values as shown in the figures. Solid lines are theoretical curves and marker points indicate simulation curves.

shown in Figure 10 are the theoretical curves given by

$$\frac{\sigma}{\sigma_{\delta_c}} = \frac{E_f \epsilon_y \cos^2 \bar{\alpha}}{\sigma_{\delta_c}} = \frac{E_f \epsilon_y \cos^2 \bar{\alpha}}{\sigma_{\delta}} \left(\frac{\delta}{\delta_c} \right)^{1/\rho},$$

where it is assumed that all the fibers have the same helix angle $\bar{\alpha}$ given by

$$\bar{\alpha} = \cos^{-1} \left(\frac{\sum_{k=1}^l n_k \cos \alpha_k}{n} \right).$$

We achieve very good agreement between the theoretical and simulation curves, except for large values of α_s , where localized failure mechanisms might come into play. These plots correspond to a single realizations of a yarn test and thus conclusions cannot be drawn regarding the relative strengths and strains to failure for different values of ρ and α_s because the yarn realizations exhibit variability from one to another.

3.4. Cumulative probability distribution, mean and standard deviation. Figure 11 shows the cumulative probability distribution functions, G , resulting from the Monte Carlo simulations for $\alpha_s = 10^\circ$ and $\rho = 2, 5, \text{ and } 10$ on normal probability paper. The nearly straight lines indicate that the strength is approximately normally distributed.

Figure 12 and 13 plot the normalized mean strength, $\mu/\sigma_{\delta_c^{\min}}$, and standard deviation, $\sqrt{n} \gamma/\sigma_{\delta_c^{\min}}$, versus surface helix angle, α_s , for $n = 62$ and 279 , and $\rho = 2, 5, \text{ and } 10$ (for $f = 0.1$ and 0.3). In these calculations we use δ_c^{\min} as the yarn characteristic length. Significantly, the curves for the two values of friction coefficients, that is, $f = 0.1$ and 0.3 coincide with each other when normalized with respect to $\sigma_{\delta_c^{\min}}$. For comparison, we also show the results from the earlier work [Porwal et al. 2006] on TM-ELS. The TM-GLS and TM-ELS curves generally exhibit the same behavior for δ_c^{\min} . The TM-GLS curves, however, show some improvement in the strength due the presence of frictional forces. As in the TM-ELS bundle, the TM-GLS bundles also exhibit a size effect. The strength is slightly lower for a larger bundle with $n = 279$ fibers than for smaller one with $n = 62$. No particular pattern in the standard

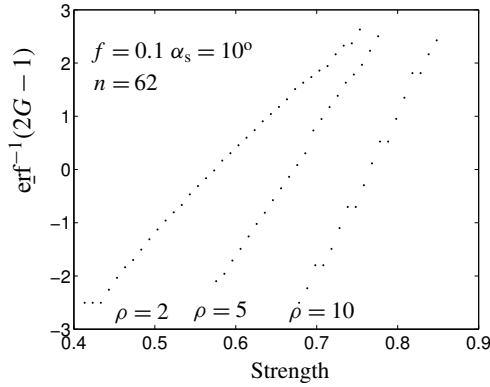


Figure 11. Cumulative probability distribution function on normal probability paper ($n_s = 10000$).

deviation is seen apart from the fact that it decreases with an increase in ρ corresponding to a decrease in fiber strength variability. Further study is required to exactly understand the size effects and the standard deviation in the strength of these twisted yarns.

3.5. Effect of length scale on strength development and existence of optimal twist angle. Figure 14 clearly indicates the importance of the choice of δ_c , by comparing the mean strength of the yarns with surface twist α_s for different choices of simulation lengths, δ_c^{\max} , δ_c^{\min} , or δ_c^{avg} . When mean bundle strength is simply normalized by μ_1 , the mean bundle strength at $\alpha_s = 1^\circ$, it increases with surface twist angle α_s , up to $\alpha_s = 25^\circ$. However, normalizing by μ_1 is not completely correct because it does not account for the size effect in the strength of the individual fibers. The scale parameter of the individual fibers increases, as δ_c decreases, according to

$$\sigma_{\delta_c} = \left(\frac{\delta_0}{\delta_c}\right)^{1/\rho} \sigma_{\delta_0}.$$

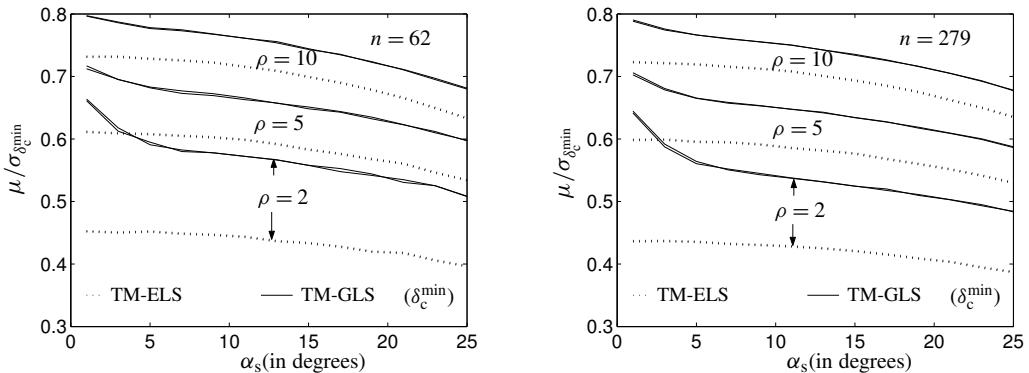


Figure 12. Normalized mean, $\mu/\sigma_{\delta_c^{\min}}$, versus surface helix angle, α_s . The TM-GLS results are for $f = 0.1$ and 0.3 . TM-ELS results are from [Porwal et al. 2006].

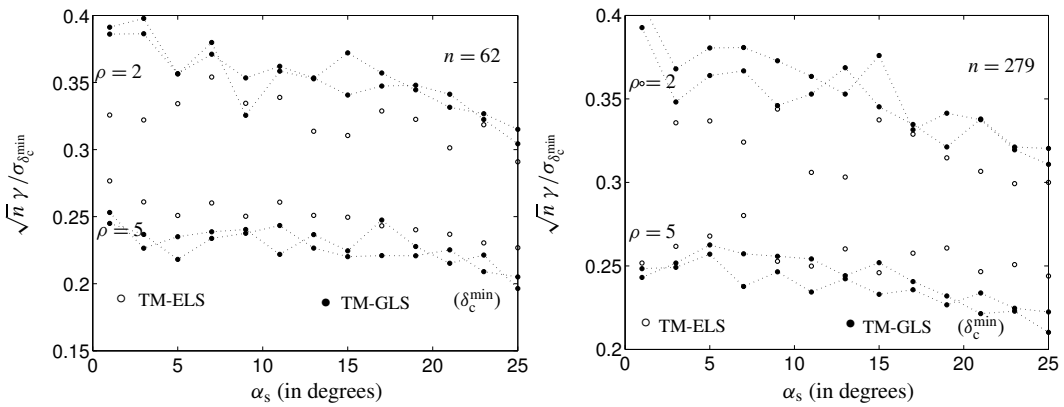


Figure 13. Normalized standard deviation $\sqrt{n} \gamma / \sigma_{\delta_c^{\min}}$ versus surface helix angle α_s . The TM-GLS results are for $f = 0.1$ and 0.3 . TM-ELS results are from [Porwal et al. 2006].

This more appropriate normalization will account for the changing length of the bundle in simulation. Significantly, the yarn strength achieves a maximum for δ_c^{\max} but not the other two length scales. This same result occurs with other parameter sets as well. The other two length scales limit the role played by the frictional stresses and therefore are not wise choices for modeling and simulation of yarn failure.

The inset figure in Figure 14 plots normalized bundle strength (S/S_0 , where S_0 is the bundle strength when $\alpha_s = 0^\circ$) versus surface twist angle using data extracted from experimental results of Rao and Farris [2000]. The optimal helix angle predicted by our model ($\alpha_s \approx 7^\circ$) is in excellent agreement with

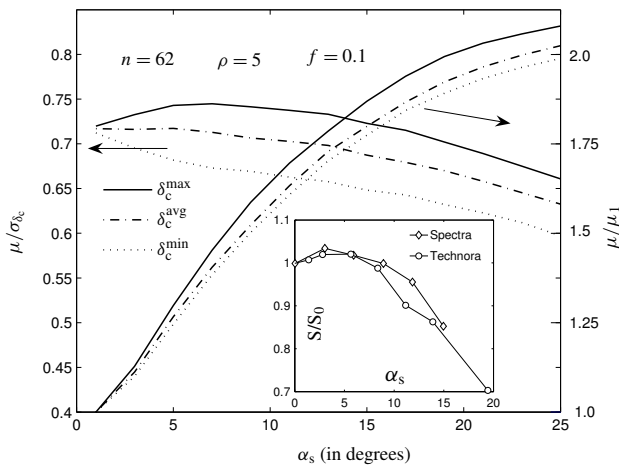


Figure 14. Normalized mean bundle strength μ / σ_{δ_c} and μ / μ_1 versus surface helix angle α_s for different length scales. Here μ_1 is the value at $\alpha_s = 1^\circ$. Inset figure (S/S_0 versus α_s) is plotted using data from [Rao and Farris 2000], where S_0 is the yarn strength when $\alpha_s = 0^\circ$.

experimental results of Rao and Farris [2000] despite the fact that the idealized yarn geometry of our model is different from the yarn produced by their twisting process. The magnitudes of the strengths are apparently different because the normalizations used are different. Further, the experimental strength decreases at relatively higher rate than theoretical value because of the inefficiencies due to incomplete migration at higher twist angle, which is assumed to be complete in our model.

4. Conclusions

We have made a fundamental improvement in the twisted bundle strength model by incorporating effects of friction and pressure development. We have defined and shown that the choice of the characteristic length scale and normalization parameter are crucial in simulating the strength behavior, particularly as a function of the surface helix angle (Figure 14). Monte Carlo simulation is employed to show that the bundle strength approximately follows a normal distribution. Further, the TM-GLS bundle strength exhibits a peak when δ_c^{\max} and $\sigma_{\delta_c}^{\max}$ are selected as the characteristic length scale and normalization parameter, respectively. In this case, broken fibers in any layer are allowed to develop stress via frictional forces to the maximum level determined by yarn extension and therefore potentially break again elsewhere along their length.

References

- [Andrews et al. 1999] R. Andrews, D. Jacques, A. M. Rao, T. Rantell, F. Derbyshire, Y. Chen, J. Chen, and R. C. Haddon, “Nanotube composite carbon fibers”, *Appl. Phys. Lett.* **75**:9 (1999), 1329–1331.
- [Barber et al. 2005] A. H. Barber, I. Kaplan-Ashiri, S. R. Cohen, R. Tenne, and H. D. Wagner, “Stochastic strength of nanotubes: an appraisal of available data”, *Compos. Sci. Technol.* **65**:15-16 (2005), 2380–2384.
- [Ericson et al. 2004] L. M. Ericson, H. Fan, H. Peng, V. A. Davis, W. Zhou, J. Sulpizio, Y. Wang, R. Booker, J. Vavro, C. Guthy, A. N. G. Parra-Vasquez, M. J. Kim, S. Ramesh, R. K. Saini, C. Kittrell, G. Lavin, H. Schmidt, W. W. Adams, W. E. Billups, M. Pasquali, W.-F. Hwang, R. H. Hauge, J. E. Fischer, and R. E. Smalley, “Macroscopic, neat, single-walled carbon nanotube fibers”, *Science* **305**:5689 (2004), 1447–1450.
- [Hearle et al. 1969] J. W. S. Hearle, P. Grosberg, and S. Vacker, *Structural mechanics of fibers, yarns, and fabrics*, vol. 1, Wiley-Interscience, 1969.
- [Huemmerich et al. 2004] D. Huemmerich, T. Scheibel, F. Vollrath, S. Cohen, U. Gat, and S. Ittah, “Novel assembly properties of recombinant spider dragline silk proteins”, *Curr. Biol.* **14**:22 (2004), 2070–2074.
- [Jiang et al. 2002] K. Jiang, Q. Li, and S. Fan, “Nanotechnology: spinning continuous carbon nanotube yarns”, *Nature* **419**:6909 (2002), 801–801.
- [Ko et al. 2003] F. Ko, Y. Gogotsi, A. Ali, N. Naguib, H. Ye, G. L. Yang, C. Li, and P. Willis, “Electrospinning of continuous carbon nanotube-filled nanofiber yarns”, *Adv. Mater.* **15**:14 (2003), 1161–1165.
- [Lazaris et al. 2002] A. Lazaris, S. Arcidiacono, Y. Huang, J.-F. Zhou, F. Duguay, N. Chretien, E. A. Welsh, J. W. Soares, and C. N. Karatzas, “Spider silk fibers spun from soluble recombinant silk produced in mammalian cells”, *Science* **295**:5554 (2002), 472–476.
- [Naik et al. 2001] N. K. Naik, I. Mudzingwa, and M. N. Singh, “Effect of twisting on tensile failure of impregnated yarns with broken filaments”, *J. Compos. Technol. Res.* **23**:3 (2001), 225–234.
- [Pan 1993] N. Pan, “Prediction of statistical strengths of twisted fibre structure”, *J. Mater. Sci.* **28**:22 (1993), 6107–61114.
- [Pan et al. 1998] N. Pan, H. C. Chen, J. Thompson, M. K. Inglesby, and S. H. Zeronian, “Investigation on the strength-size relationship in fibrous structures including composites”, *J. Mater. Sci.* **33**:10 (1998), 2667–2672.
- [Phoenix 1979] S. L. Phoenix, “Statistical theory for the strength of twisted fiber bundles with applications to yarns and cables”, *Text. Res. J.* **49**:7 (1979), 407–423.

- [Phoenix and Beyerlein 2000] S. L. Phoenix and I. J. Beyerlein, "Statistical strength theory for fibrous composite materials", Chapter 1.19, pp. 559–640 in *Comprehensive composite materials*, vol. 1, edited by A. Kelly et al., Pergamon/Elsevier, 2000.
- [Porwal et al. 2006] P. K. Porwal, I. J. Beyerlein, and S. L. Phoenix, "Statistical strength of a twisted fiber bundle: an extension of Daniels equal-load-sharing parallel bundle theory", *J. Mech. Mater. Struct.* **1**:8 (2006), 1425–1447.
- [Rao and Farris 2000] Y. Rao and R. J. Farris, "A modeling and experimental study of the influence of twist on the mechanical properties of high-performance fiber yarns", *J. Appl. Polym. Sci.* **77**:9 (2000), 1938–1949.
- [Sullivan 1942] R. R. Sullivan, "A theoretical approach to the problem of yarn strength", *J. Appl. Phys.* **13**:3 (1942), 157–167.
- [Vigolo et al. 2000] B. Vigolo, A. Pénicaud, C. Coulon, C. Sauder, R. Pailler, C. Journet, P. Bernier, and P. Poulin, "Macroscopic fibers and ribbons of oriented carbon nanotubes", *Science* **290**:5495 (2000), 1331–1334.
- [Zhang et al. 2004] M. Zhang, K. R. Atkinson, and R. H. Baughman, "Multifunctional carbon nanotube yarns by downsizing an ancient technology", *Science* **306**:5700 (2004), 1358–1361.

Received 6 Jul 2006. Revised 6 Jun 2006. Accepted 20 Feb 2007.

PANKAJ K. PORWAL: pkp2@cornell.edu

Department of Theoretical and Applied Mechanics, Cornell University, Ithaca, NY 14853

<http://www.tam.cornell.edu/~pkp2/>

IRENE J. BEYERLEIN: irene@lanl.gov

Theoretical Division, Los Alamos National Laboratory, Los Alamos, NM 87545

STUART LEIGH PHOENIX: slp6@cornell.edu

Department of Theoretical and Applied Mechanics, Cornell University, Ithaca, NY 14853

<http://www.tam.cornell.edu/Phoenix1.html>

